Numerical Investigation of Two-Dimensional H_2-Air Flameholding over Ramps and Rearward-Facing Steps

Thomas R. A. Bussing* and Earll M. Murman†
Massachusetts Institute of Technology, Cambridge, Massachusetts

The time-dependent Navier-Stokes equations, including the effects of finite rate chemistry, are numerically integrated to predict the steady-state behavior of several model supersonic flameholders. The conservation equations governing chemically reacting flows are solved using a technique based on the idea of rescaling the equations in time such that all convective and chemical processes evolve on similar "pseudo" time scales. To accomplish this, the conservation equations are preconditioned to remove the stiffness associated with these equations. The method can be used to compute the steady-state solution very efficiently, regardless of whether the flow is frozen, finite rate, or in equilibrium. Two candidate supersonic flameholders are analyzed to assess their operating characteristics. The geometries include a ramp and a rearward-facing step. All flows consider a premixed H_2-airstream and use the global chemistry model of Rogers and Chinitz. Several different kinds of flowfields are generated, depending on the level of heat release.

Introduction

THE recent interest in air-breathing, hydrogen-burning, hypersonic vehicles has created a need for efficient propulsion systems. One of the propulsion concepts envisioned for such a vehicle is based on supersonic combustion ramjets. The engines use the forward motion of the vehicle to compress the external air to low supersonic speeds where hydrogen can be injected and burned. The combustion process occurs supersonically.

Problems that must be overcome for the combustion concept to be viable are flame ignition and flameholding. Considerable work has been done in this area.[1,2] One promising concept for igniting and stabilizing a flame is an oblique shock wave. Recently, oblique shock waves[3] have even been proposed for a hypersonic engine concept called an oblique detonation wave engine (ODWE). Another device that can act as a flame ignitor/flameholder is a rearward-facing step. In this article, both the oblique shock and rearward-facing step geometries will be analyzed numerically to assess their flame ignition and flameholding properties.

Governing Equations

The conservation equations governing viscous, laminar two-dimensional flows with chemical reaction can be written as

$$\frac{\partial U}{\partial t}+\frac{\partial F}{\partial x}+\frac{\partial G}{\partial y}+H=0 \tag{1}$$

The vectors U, F, G, and H are

$$U=(\rho,\rho u,\rho v,\rho E,\rho Y_k)^T \qquad H=(0,0,0,0,-\dot{w}_k)^T$$

$$F=\begin{bmatrix}\rho u\\ \rho u^2+\sigma_{xx}\\ \rho uv+\tau_{xy}\\ \rho Eu+u\sigma_{xx}+v\tau_{yx}+q_x\\ \rho Y_k u-\Gamma Y_{kx}\end{bmatrix}$$

$$G=\begin{bmatrix}\rho v\\ \rho uv+\tau_{yx}\\ \rho v^2+\sigma_{yy}\\ \rho Ev+v\sigma_{yy}+u\tau_{xy}+q_y\\ \rho Y_k v-\Gamma Y_{ky}\end{bmatrix} \tag{2}$$

where Y_k is the kth species density fraction and $\dot{w}_k$ is the kth species source term. The various quantities can be written as

$$\sigma_{xx}=p-\lambda(u_x+v_y)-2\mu u_x \tag{3}$$

$$\tau_{xy}=-\mu(u_y+v_x)=\tau_{yx} \tag{4}$$

$$\sigma_{yy}=p-\lambda(u_x+v_y)-2\mu v_y \tag{5}$$

$$q_x=-\kappa\frac{\partial T}{\partial x}-\Sigma\frac{\mu}{Pr}Hf_k\frac{\partial y_k}{\partial x} \tag{6}$$

$$q_y=-\kappa\frac{\partial T}{\partial y}-\Sigma\frac{\mu}{Pr}Hf_k\frac{\partial y_k}{\partial y} \tag{7}$$

$$\lambda=-\tfrac{2}{3}\mu \tag{8}$$

$$\kappa=\text{thermal conductivity} \tag{9}$$

$$\Gamma=\frac{\mu}{Sc}=\frac{\mu}{Pr}\quad(Le=1) \tag{10}$$

Presented as Paper 85-1250 at the AIAA/SAE/ASME/ASEE 21st Joint Propulsion Conference, Monterey, CA, July 8–10, 1985; received April 7, 1986; revision received June 9, 1987.

*Research Assistant; presently Principal Engineer at Boeing Military Airplane Co. Member AIAA.

†Professor, Department of Aeronautics and Astronautics. Fellow AIAA.

Pr, *Sc*, and *Le* are the Prandtl, Schmidt, and Lewis numbers, respectively. Finally, to close the equation set, the total energy and the equation of state are given as

$$E=\sum_k Y_k\int_0^T Cv_k\,dT+\frac{u^2+v^2}{2}+\sum_k Hf_k Y_k \tag{11}$$

$$P=\frac{\rho R^\theta T}{Aw} \tag{12}$$

where Hf_k is heat of formation for species k, R^θ the universal gas constant, Aw the molecular weight, Ns the number of species, and k varies from 1 to $Ns-1$. The laminar viscosity is calculated from Sutherland's law.

$$\mu_{\text{laminar}}=\frac{1.458\times10^{-6}T^{3/2}}{(T+110.33)}\ \text{kg/m}-\text{s} \tag{13}$$

H_2-Air Combustion Model

The hydrogen-air combustion model used in this study was proposed by Rogers and Chinitz[4] in 1982. The model was developed to represent H_2-air combustion kinetics in a scramjet combustor with as few reaction steps and species as possible. The model consists of the following two steps:

$$\begin{aligned}&H_2+O_2 \underset{K_{b1}}{\overset{K_{f1}}{\langle\!=\!=\!\rangle}} 2\ OH\\ &2\ OH+H_2 \underset{K_{b2}}{\overset{K_{f2}}{\langle\!=\!=\!\rangle}} 2\ H_2O\end{aligned} \tag{14}$$

where the forward reaction rate constants K_{f1} and K_{f2} are given by

$$K_{fi}=A_i(\phi)T^{Ni}\exp(-E_i/R^\theta T) \tag{15}$$

$A_i(\phi)$ is a function of the equivalence ratio ϕ, defined as the fuel-to-air ratio divided by the stoichiometric fuel-to-air ratio. Values of the parameters used in this model are:

$$A_1(\phi)=\left(8.917\phi+\frac{31.433}{\phi}-28.950\right)\times10^{47}\ \text{cm}^3/\text{mole}-\text{s}$$

$$A_2(\phi)=\left(2.000+\frac{1.333}{\phi}-0.883\phi\right)\times10^{64}\ \text{cm}^6/\text{mole}^2-\text{s}$$

$$E_1=4865\ \text{cal/mole}$$

$$E_2=42{,}000\ \text{cal/mole}$$

$$N_1=-1$$

$$N_2=-13$$

$$R=1.987\ \frac{\text{cal}}{\text{mole}-\text{K}} \tag{16}$$

The backward reaction rates are given by

$$K_{b1}=\frac{K_{f1}}{K_{eq_1}} \tag{17}$$

and

$$K_{b2}=\frac{K_{f2}}{K_{eq_2}} \tag{18}$$

where K_{eq_1} and K_{eq_2} are the equilibrium constants for each reaction.

The model is valid for temperatures between 1000 and 2000 K and equivalence ratios between 0.1 and 2.0. Because the chemistry model is not valid below a temperature of 1000 K, an ignition temperature must be specified. In this study, the ignition temperature is equal to 1000 K unless otherwise specified. The reaction rates for the various species conservation equations can be written as

$$\dot{w}_k=\dot{C}_k Aw_k \tag{19}$$

where the $\dot{C}_k$ (mole/cm^3 – s) for the Rogers/Chinitz model are

$$\dot{C}_{O_2}=[K_{f1}C_{H_2}C_{O_2}+K_{b1}(C_{OH})^2] \tag{20}$$

$$\dot{C}_{H_2O}=2[-K_{f2}C_{H_2}(C_{OH})^2-K_{b2}(C_{H_2O})^2] \tag{21}$$

$$\dot{C}_{H_2}=(\dot{C}_{O_2}-\tfrac{1}{2}\dot{C}_{H_2O}) \tag{22}$$

$$\dot{C}_{OH}=-(2\dot{C}_{O_2}+\dot{C}_{H_2O}) \tag{23}$$

Aw_k is the kth species molecular weight, and the C are related to the Y through the following equation:

$$C_k=\frac{\rho Y_k}{Aw_k} \tag{24}$$

Finally, to close the equation set, a relation can be written for the sum of the species density fractions,

$$Y_{H_2}+Y_{O_2}+Y_{OH}+Y_{H_2O}+Y_{N_2}=1 \tag{25}$$

N_2 is present in the calculations, but is assumed to be inert.

Numerical Method

The numerical integration of the equations governing chemical reacting flows can be very expensive unless special care is taken to remove the time stiffness limitations characteristic of these problems. A variety of numerical methods has been developed to solve these equations, including both explicit and implicit techniques.[5] Purely explicit methods are limited and become very inefficient when the time scales associated with chemical reaction become small compared to the fluid time scales. Implicit methods overcome these limitations but lose their high performance when applied to problems with more than one space dimension.

A preconditioning procedure was developed[6] that successfully removes the stiffness limitations due to chemical reactions and whose performance does not degrade when applied to problems with more than one space dimension. In addition, the preconditioning technique can be applied to multiple grid acceleration methods,[6] which can further improve the efficiency of the scheme. The basic idea is to modify the original unsteady equation (1) to

$$S\frac{\partial U}{\partial t}=-\frac{\partial F}{\partial x}-\frac{\partial G}{\partial y}-H \tag{26}$$

S is a preconditioning matrix used to rescale the equations in time so that each quantity in the state vector U is numerically advanced at its own characteristic rate. Specifically, this means that a fluid quantity is marched at a fluid time scale and a species quantity at its own chemical rate time scale. Note that both equations satisfy the same steady-state equa-

tion. If only the steady-state solution is desired, then advancing each state quantity at its own characteristic rate produces a time-inaccurate solution, but one that converges very quickly. With this particular technique, the number of iterations needed to achieve steady state is found to be independent of the level of stiffness. Stiffness is defined as the ratio of the largest to the smallest eigenvalue of the system of discrete equations. A similar but more convenient definition used in this article is the ratio of the convective fluid time scale (based on the computational cell dimension) to the chemical reaction time scale,

$$S = \frac{\tau_{\text{fluid}}}{\tau_{\text{chem}}} \tag{27}$$

For the problems of interest, S can vary from 0 to 10^6, which can translate into substantial computational work savings. If a time-accurate solution is desired, then one need only reduce the numerical time step to the time scale of interest. In addition, the use of a local CFL number can improve the rate of convergence of the scheme. The details of this method can be found in Refs. 6 and 7.

The preconditioning procedure is applied to the Jameson, Schmidt, and Turkel finite-volume scheme. A description of the method used to evaluate the viscous terms is given in Refs. 7 and 8. The accuracy of the method has been verified in comparisons with analysis and experiment for inviscid compression ramps, a laminar flat-plate boundary layer, and a rearward-facing step.

Results for Two-Dimensional Flow with H_2-Air Chemistry

Inviscid Compression Ramp

In this section, a class of 10-deg compression ramp flameholders will be investigated. The geometry was chosen because it can generate an oblique shock of sufficient strength to ignite and hold a reaction zone. The flowfield will be simulated using the two-dimensional Euler equations with the Roger and Chinitz[4] chemistry model. Neglecting the viscous diffusion terms means that there are no laminar diffusion flame effects in this problem. For the inviscid calculations, the combustion zone will be referred to as a reaction zone. In the next section, where the viscous terms are included in the computations, the combustion zone will be referred to as a flame. The remainder of this section will be devoted to studying the effects of combustion and heat release on the flowfield. In particular, it will be shown how the flowfield character can be changed from a fully supersonic flow to one with embedded subsonic zones or to a fully subsonic flowfield. The ability to predict all three types of flows is of interest in scramjet design.

The baseline condition, case I, corresponds to the flameholder geometry shown in Fig. 1, and to the flow and chemistry parameters of Tables 1 and 2. Three other cases correspond to perturbing one of the parameters from this baseline. In all cases considered, premixed hydrogen and air enter the channel at Mach number 2.5. The incoming flow variables u, v, T, and ρ were held fixed at the values set in Table 1. Zero mass flux boundary conditions were used to model the upper and lower walls of the channel. The flow at the channel exit was assumed to be supersonic, and first-order accurate extrapolation was used for outflow boundary conditions. The Mach number and H_2O density fraction contours for the baseline condition (case I) are shown in Figs. 2 and 3, respectively. The temperature increase through the oblique shock wave generated by the compression ramp exceeds the ignition temperature. It can be seen from the H_2O contours that the oblique shock triggers combustion and that the reaction zone thickness is approximately 0.2 of the channel length. It can also be seen from these figures that the oblique shock undergoes a regular reflection from the lower channel wall and that the expansion fan from the corner of the ramp does not interfere with either the oblique shock or the reaction zone. For this baseline condition, the flow is supersonic throughout the channel.

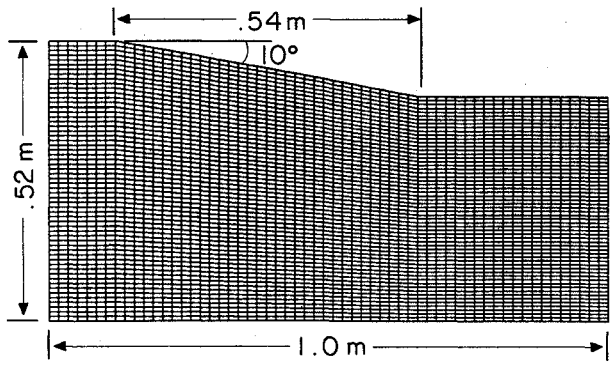

Fig. 1 Baseline compression ramp geometry and 60×60 computational grid.

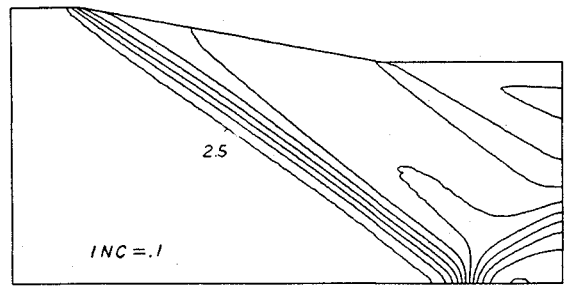

Fig. 2 Mach number contours for baseline compression ramp flameholder—case I, $\phi = 0.1$.

Table 1 Data for H_2-air calculations

Property	Dimensions	Values	
		2-D Ramp	2-D Step
P_∞	N/m^2	1.0×10^5	1.0×10^5
T	K	900	900
T_{ignition}	K	1000	1300
ϕ		0.1	0.5
M_∞		2.5	2.0
U_∞	m/s	1500	1200
V_∞	m/s	0	0.0
Re_H			230,000
Pr			1.0

Table 2 Chemistry data for H_2O-air calculations

Property	Dimensions	Value
C_{pH2O}	J/kg K	17160
C_{pOH}	J/kg K	1181
C_{pH2}	J/kg K	2854
C_{pO2}	J/kg K	2041
C_{pN2}	J/kg K	1285
C_{VH2O}	J/kg K	17160
C_{VOH}	J/kg K	1181
C_{VH2}	J/kg K	2854
C_{VO2}	J/kg K	2041
C_{VN2}	J/kg K	1285
Hf_{H2O}	J/kg	-1.44×10^7
Hf_{OH}	J/kg	2.3×10^6
Hf_{H2}	J/kg	0.0
Hf_{O2}	J/kg	0.0
Hf_{N2}	J/kg	0.0

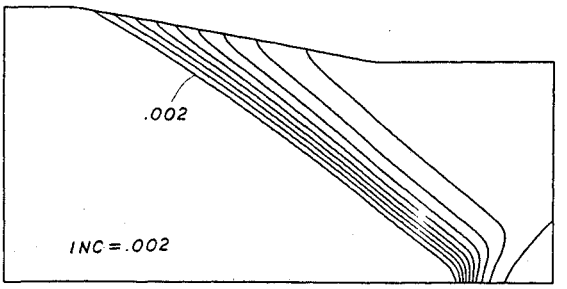

Fig. 3 H_2O density fraction contours for baseline compression ramp flameholder—case I, $\phi = 0.1$.

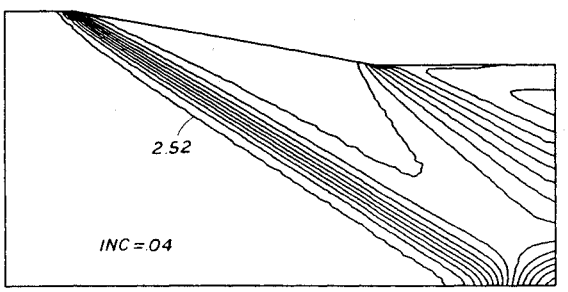

Fig. 4 Mach number contours for case II, $\phi = 0.1$. Reaction has been artificially suppressed.

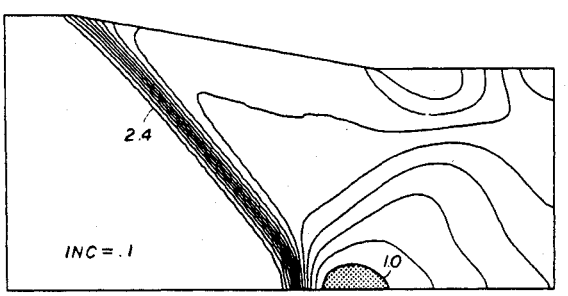

Fig. 5 Mach number contours for case II, $\phi = 0.24$. Shaded area indicates subsonic Mach number.

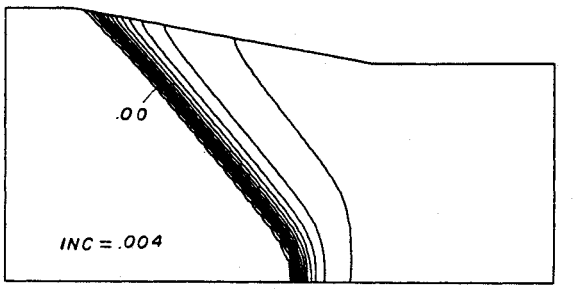

Fig. 6 H_2O density fraction contours for case II, $\phi = 0.24$.

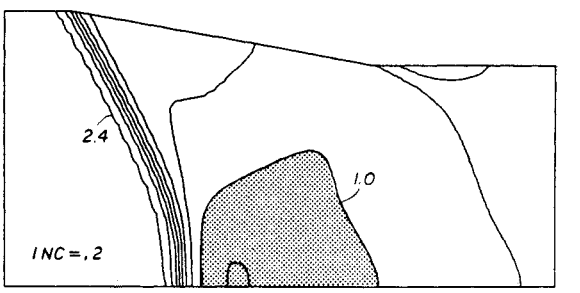

Fig. 7 Mach number contours for case II, $\phi = 0.35$. Shaded area indicates subsonic Mach number.

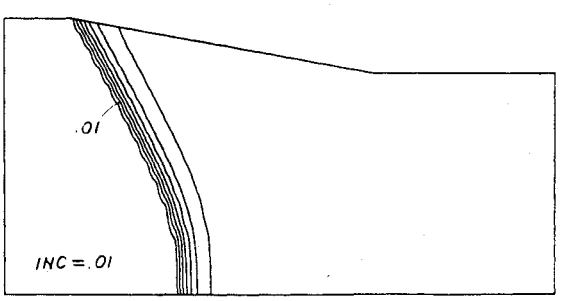

Fig. 8 H_2O density fraction contours for case II, $\phi = 0.35$.

For case II, the equivalence ratio ϕ is varied to observe the effects of heat release on the flowfield. Figure 4 shows the Mach number distribution for the baseline condition but with no reaction. The equivalence ratio $\phi = 0.1$, but the combustion is artificially suppressed. It can be seen that with no heat release, the oblique shock is further downstream than in Fig. 2, intersecting the lower wall approximately 10% further aft. The Mach number behind the shock, as well as behind the corner expansion fan, is higher in Fig. 4 than in the reacting flow of Fig. 2. The remaining examples in this section show the effects of increasing heat release. Figures 5 and 6 present the Mach number and the H_2O density fraction distribution for $\phi = 0.24$. This increased level of heat release produces a normal shock wave followed by a small embedded subsonic zone adjacent to the lower wall. Increasing the equivalence ratio to $\phi = 0.35$ produces the results shown in Figs. 7 and 8. The subsonic region has grown in size, and the shock wave has moved forward approximately 50% of the channel length from the baseline case. A minimum Mach number of 0.79 is reached in the channel.

If the value of ϕ is increased still further, then the heat release is high enough to choke the flow thermally. Thermal choking appears to correspond to the embedded subsonic zone extending from the lower to the upper wall, and a normal shock wave is formed. Although there may be a stable region with the normal shock in the channel, for the calculations performed, the shock moved to the upstream boundary of the computational domain. Since the boundary conditions enforced a supersonic inflow, the shock was artificially held at this position. An example of this calculation is given in Ref. 7.

Case III considers the effect of changing the flameholder length scale while holding all other parameters constant at the baseline condition. Specifically, the channel length and height are reduced to one-tenth of the dimensions shown in Fig. 1, while the same values are kept for the parameters in Tables 1 and 2. This has the effect of making the reaction zone thickness much larger than the channel length. The Mach number and H_2O density fraction contours are shown in Figs. 9 and 10. The oblique shock position and strength of Fig. 9 correspond to the nonreacting conditions of Fig. 4. A comparison of the H_2O density fraction contours for this case (Fig. 10) with those of the baseline case (Fig. 3) illustrates that the thickness of the reaction zone is much larger than the ramp length and that most of the combustion and heat release occurs downstream of the channel. Although the reaction does affect the strength of the corner expansion fan, the limited heat release has only a weak effect on the flow compared to the baseline case. This example serves to illustrate that care must be taken to match the reaction-zone length scale and that of the flameholder geometry to produce the desired behavior.

In the final inviscid example, case IV, the interaction of the corner expansion fan with the oblique shock and reaction zone is illustrated by reducing the compression ramp length. The geometry illustrated in Fig. 11 shows that the ramp length has been reduced to 37% of the baseline value while all other parameters have been held fixed at the baseline values. Figures 12–14 show the contours of Mach number, H_2O density fraction, and H_2O reaction rate. These figures illustrate that the reaction zone is limited to a small region. The corner expansion fan weakens the shock and quenches the reaction. The reaction rate contours show where H_2O is actually being produced. Some of these same effects can also be seen in case III (Fig. 10).

The above results illustrate that a variety of flow patterns can be produced due to the coupling between the heat release due to combustion and the compressible flow. There are a variety of parameters, including Mach number, ϕ, channel geometry, and chemistry model. It will be helpful for the designer if a way can be found to characterize or categorize the effect of these parameters in a graphical form. One possible way of doing this, suggested by these and many other examples in this study, is contained in Ref. 7.

Laminar Flow for Rearward-Facing Step

Flameholding occurs when a chemical reaction is initiated in a flowfield and a stable flame propagates downstream from the point. In a viscous flow near a solid wall, flameholding can occur in two ways. The first way is to have a flow with a maximum temperature above the ignition temperature. In this case, combustion will always occur. In the second situation, the maximum temperature reached in the flow is everywhere below the fuel ignition temperature. For burning to occur, an ignition source must be provided. Only under certain situations, however, can a stable flameholder be produced.

One example of a possible supersonic flameholder in which viscous effects are important is a rearward-facing step. These devices operate by creating a hot spot behind the step from which heat and radicals can diffuse into the unburned mixture. If the fluid maximum temperature is above the fuel ignition temperature and a premixed flow is considered, the step offers little benefit since the boundary layer before and after the step will also be reacting. For this case, a stable flameholder could be produced as long as the flow is not thermally choked. If the fluid maximum temperature is everywhere below the fuel ignition temperature, the step can provide a volume of hot gas from which heat and radicals can diffuse out, to ignite the unburned gas mixture coming over the step. To get the flow burning in this case, an ignition source must be provided. For a stable flameholder to exist, the heat produced in the recirculation zone must be equal to the heat that diffuses out of the recirculation zone. This implies that a fluid particle must remain in the recirculation long enough for chemical reaction to occur.

In this section, an attempt will be made to characterize the rearward-facing step geometry. The full two-dimensional, laminar Navier-Stokes equations with H_2-air chemistry will be solved using the chemical time-scaled preconditioned Jameson, Schmidt, and Turkel scheme with the constant CFL condition. For these calculations, the flow over the step was assumed to be premixed.

The computational mesh used for all the rearward-facing step calculations is shown in Fig. 15, while the fluid and chemistry data are given in Tables 1 and 2. Note that the lower boundary is modeled as a solid wall and that the upper wall is modeled as a symmetry line. In order to reduce the computational domain size, an incompressible Blasius flat-plate boundary-layer profile was specified at the inlet. For this example, the solid walls were assumed to be adiabatic and noncatalytic. The validation of the code for nonreacting rearward-facing step flows is given in Ref. 7.

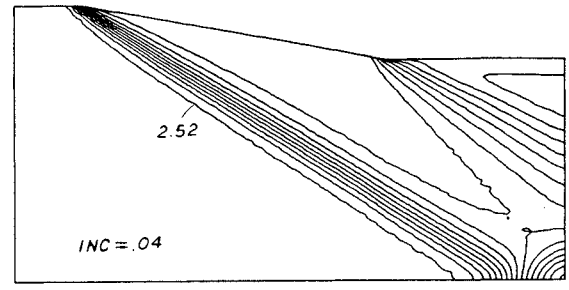

Fig. 9 Mach number contours for case III, reduced channel dimensions.

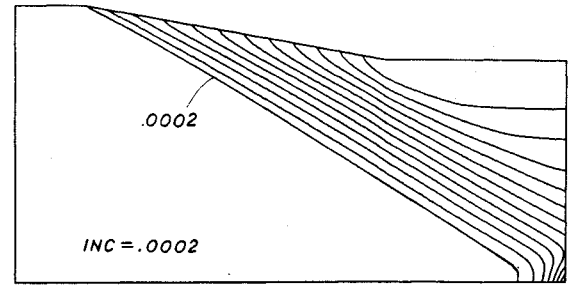

Fig. 10 H_2O density fraction contours for case III, reduced channel dimensions.

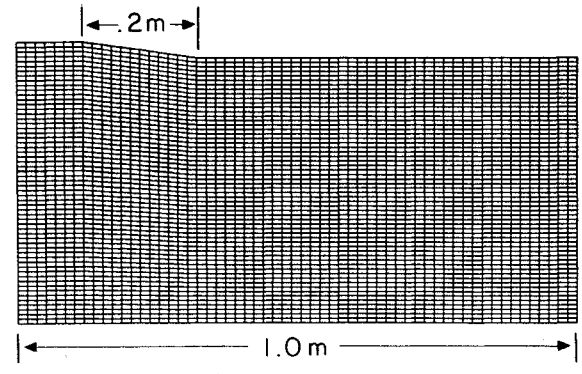

Fig. 11 Short ramp geometry and grid, case IV.

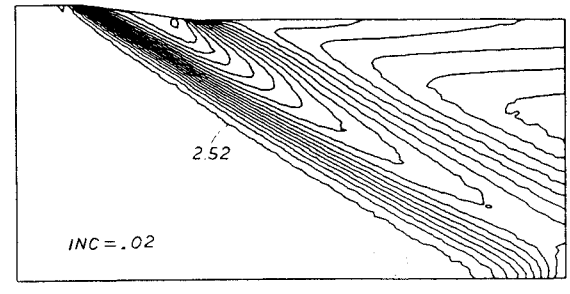

Fig. 12 Mach number contours for case IV, short ramp.

The flow over a rearward-facing step depends strongly on the ratio of the boundary-layer thickness to the step height Ω. The three interesting limits are $\Omega \gg 1$, $\Omega \simeq 1$, and $\Omega \ll 1$. In the first case, $\Omega \gg 1$, the amount of flameholding provided by the step is small compared to the flameholding provided by a simple flat-plate boundary layer. In this case, the step has little or no effect on flameholding and will not be considered further here. For $\Omega \simeq 1$, the boundary-layer thickness was chosen to be equal to the height of the step, which is typical for scramjet applications. Finally, the boundary-layer thickness was set to zero for the case when $\Omega \ll 1$.

The flow is also strongly affected by the ratio of the fluid maximum temperature to the fuel ignition temperature Σ. If $\Sigma > 1$, the fuel and air autoignite wherever the static temperature is above the fuel ignition temperature. If $\Sigma < 1$, for chemical reaction to occur, an ignition source must be provided. Numerically, this implies forcing the temperature behind the step to be above the ignition temperature for a period of time and then removing this constraint once the fuel has started burning.

Examples of a nonreacting velocity field, with $\Omega \simeq 1$, $\Sigma > 1$, and $\phi = 0.5$, are shown in Fig. 16. A blowup of the region behind the step shows clearly the recirculation region, Fig. 17. Figure 18 shows that with combustion, chemical reaction occurs in the boundary layers and behind the step. In this case, chemical reaction has increased the size of the recirculation zone and the thickness of the boundary layers. The amount of chemical reaction produced by the step is comparable to that produced by the boundary layer coming over the step. The maximum temperature reached behind the step is approximately 1850 K. If ϕ is increased to 1, the flow thermally chokes.

Using the same flow conditions just discussed but with a step height equal to 0.15 m, $\Omega = 0$, and $\phi = 0.5$, the following is generated. First the nonreacting velocity field distribution is given in Fig. 19. With combustion (Fig. 20), chemical reaction occurs behind the step, causing the recirculation zone to enlarge and the reattachment point to move further downstream. The maximum temperature reached was approximately 2350 K. In this case, chemical reaction is limited to the region behind the step. Thus if $\Sigma > 1$, the step serves only to increase the size of the burning region compared to a simple boundary layer. The increased reaction zone size could increase the rate at which heat and radicals are transferred to the unburned fluid and thus increase the rate of flame spreading away from the flameholding region.

If $\Sigma < 1$, the steady-state solution will depend on the initial conditions. To compute the stable reacting solution, if one exists, requires that an ignition source be provided. To ignite the fuel, a hot spot is created behind the step. The assumption here is that the release of heat will raise the local static temperature above the fuel ignition temperature and sustain a stable burning process. This means that a stable flame can

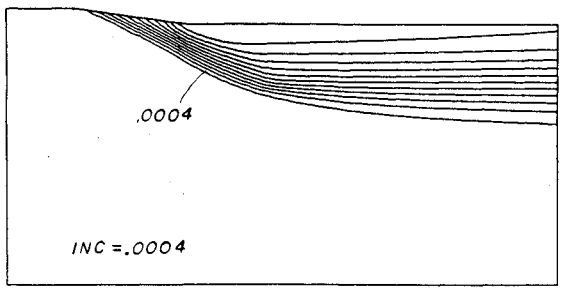

Fig. 13 H_2O density fraction contours for case IV, short ramp.

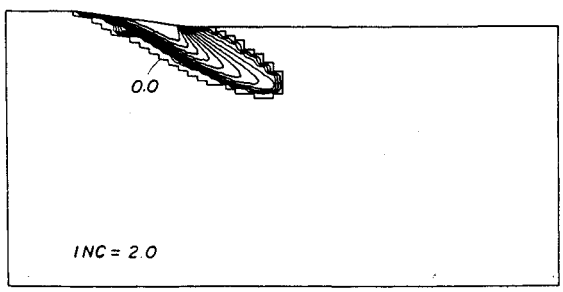

Fig. 14 H_2O reaction rate contours for case IV, short ramp.

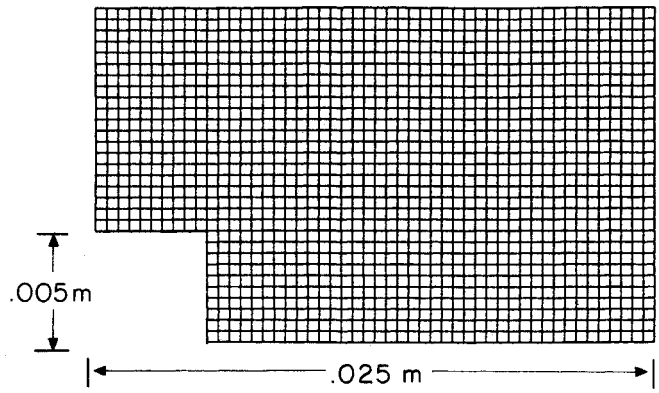

Fig. 15 Rearward-facing step geometry and 51×31 grid.

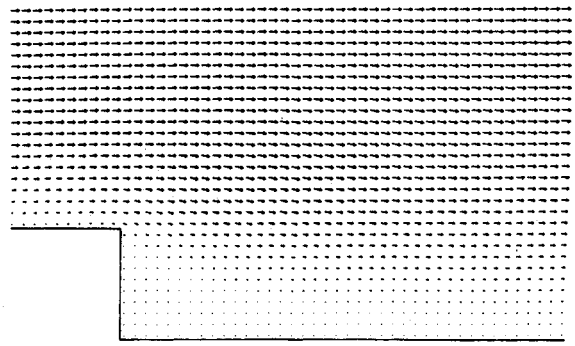

Fig. 16 Nonreacting velocity vector field: $\Omega = 1$, $\Sigma > 1$, $\phi = 0.5$. Combustion has been artificially suppressed.

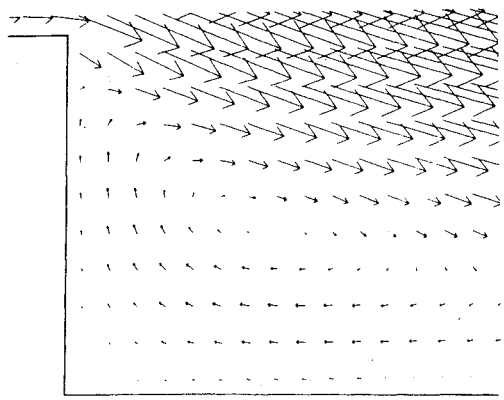

Fig. 17 Blowup of recirculation zone of Fig. 16.

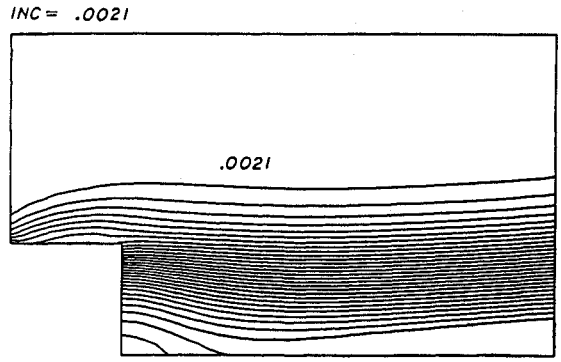

Fig. 18 H_2O density fraction contours for $\Omega = 1$, $\Sigma > 1$, $\phi = 0.5$.

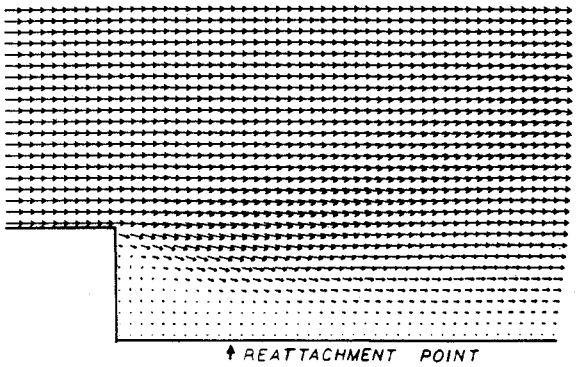

Fig. 19 Nonreacting velocity vector field, $\Omega=0$, $\Sigma>1$, $\phi=0.5$. Combustion has been artificially suppressed.

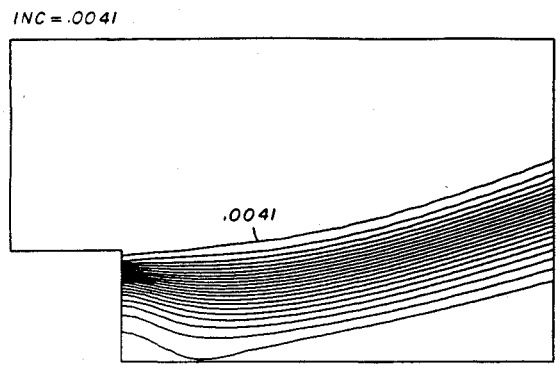

Fig. 20 H_2O density fraction contours, $\Omega=0$, $\Sigma>1$, $\phi=0.5$.

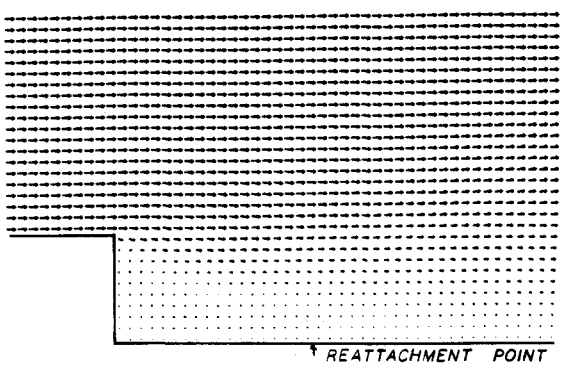

Fig. 21 Reacting velocity vector field, $\Omega=0$, $\Sigma<1$, $\phi=1.0$.

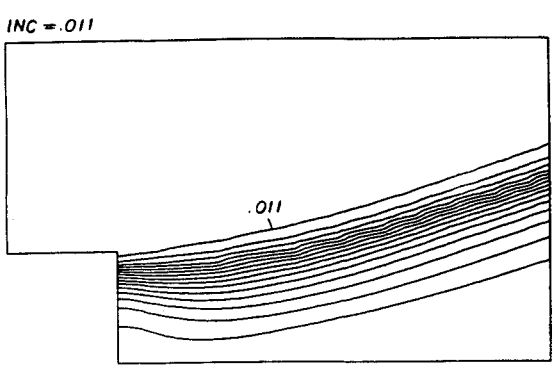

Fig. 22 H_2O density fraction contours, $\Omega=0$, $\Sigma<1$, $\phi=1.0$.

be produced only if the fuel concentration is high enough to ensure a sufficient level of heat release. For the problem under consideration, the nonreacting maximum temperature is approximately 1350 K. As a demonstration that multiple steady states are possible, consider increasing the fuel ignition temperature to 1450 K, $\Omega \ll 1$. Note that the fuel ignition temperature is usually a constant but is varied here to illustrate a point. With a $\phi=1$ and the chemistry model turned on, two different steady states can be arrived at by varying the initial conditions. The two steady states include a nonreacting and a reacting solution. If the starting temperature was chosen to be below T_{ig}, then the nonreacting solution was obtained. If a hot spot was set up behind the step, then the reacting steady-state solution was obtained. Figures 21 and 22 show the velocity field and H_2O density fraction contours for this situation. The maximum temperature reached in the flowfield was 2860 K. Note that below a minimum ϕ, only one solution can be generated, i.e., the nonreacting steady state.

It can be seen that for this rearward-facing step geometry, the equivalence ratio ϕ, boundary-layer thickness to step height ratio Ω, and maximum temperature to ignition temperature ratio Σ are all important parameters. For some values of these parameters no reaction occurs, for other values there is a stable flame, and for too much heat release the flow chokes. Again, it would be helpful to characterize these on a simple plot, and one such possibility is discussed in Ref. 7.

Conclusion

Several important contributions to the field of computational fluid dynamics and chemically reacting flows associated with supersonic flameholders can be drawn from this study and summarized as follows:

1) A preconditioning technique has been successfully applied to strongly interacting two-dimensional fluid flows with finite rate chemistry.

2) Two candidate supersonic flameholders were studied using the two-dimensional Euler and Navier-Stokes equtions with an H_2-air chemistry model.

3) With the ramp flameholder geometry, at least three different flowfields could be produced. These included fully supersonic flow, supersonic flow with an embedded subsonic zone, and a thermally choked flow.

4) The onset of thermal choking could be delayed by shortening the ramp wedge or increasing the ratio of the flame thickness to the ramp length.

5) Reacting flows over rearward-facing steps were found to be strongly dependent on the ratio of the boundary-layer thickness coming over the step to the step height and to the ratio of fluid maximum to fuel ignition temperatures.

Acknowledgments

This research was supported by NASA Langley Research Center under Grant NAG-1-229 monitored by Dr. L. Beach and G. Anderson.

References

[1]McClinton, C. R. and Jacobowski, A. K., "Parametric Investigation of Hydrogen Fueled Scramjet Flameholding," 20th JANNAF Combustion Meeting, CPIA Publ. 383, Vol. III, Oct. 1983, pp. 35-49.

[2]McClinton, C. R., "Autoignition of Hydrogen Injected Transverse to a Supersonic Airstream," AIAA Paper 79-1239, June 1979.

[3]Morrison, R. B., "Oblique Detonation Wave Ramjet," NASA CR-15344, 1980.

[4]Rogers, R. C. and Chinitz, W., "On the Use of a Global Hydrogen-Air Combustion Model in the Calculation of Turbulent Reacting Flows," AIAA Paper 82-0112, 1982.

[5]Kee, R. J. and Dwyer, H. A., "Review of Stiffness and Implicit Finite Difference Methods in Combustion Modeling," *Progress in Astronautics and Aeronautics: Combustion in Reactive Systems*, Vol. 76, edited by J. R. Bowen et al., AIAA, New York, Aug. 1979.

[6]Bussing, T. R. A. and Murman, E. M., "A Finite Volume Method for the Calculation of Compressible Chemically Reacting Flows," AIAA Paper 85-0331, Jan. 1985; to be published in *AIAA Journal*.

[7]Bussing, T. R. A., "A Finite Volume Method for the Navier-Stokes Equations with Finite Rate Chemistry," Ph.D. Thesis, Dept. of Aeronautics and Astronautics, MIT, Cambridge, MA, Aug. 1985; also MIT CFDL-TR-85-3.

[8]Swanson, R. C. and Turkel, E., "A Multistage Scheme for the Navier Stokes Equations," AIAA Paper 85-0035, Jan. 1985.